ADVANCED MATERIALS TECHNOLOGIES
www.advmattechnol.de

Self-Regulative Direct Ink Writing of Frontally Polymerizing Thermoset Polymers

Jia En Aw, Xiang Zhang, Arif Z. Nelson, Leon M. Dean, Mostafa Yourdkhani, Randy H. Ewoldt, Philippe H. Geubelle, and Nancy R. Sottos**

The ability to manufacture highly intricate designs is one of the key advantages of 3D printing. Achieving high dimensional accuracy requires precise, often time-consuming calibration of the process parameters. Computerized feedback control systems for 3D printing enable sensing and real-time adaptation and optimization of these parameters at every stage of the print, but multiple challenges remain with sensor embedment and measurement accuracy. In contrast to these active control approaches, here, the authors harness frontal polymerization (FP) to rapidly cure extruded filament in tandem with the printing process. A temperature gradient present along the filament, which is dependent on the printing parameters, can impose control over this exothermic reaction. Experiments and theory reveal a self-regulative mechanism between filament temperature and cure kinetics that allows the frontal cure speed to autonomously match the print speed. This self-regulative printing process rapidly adapts to changes in print speed and environmental conditions to produce complex, high-fidelity structures and freestanding architectures spanning up to 100 mm, greatly expanding the capabilities of direct ink writing (DIW).

1. Introduction

Capabilities for additive manufacturing of thermoset polymers and composites have grown significantly over the past two decades. Although many thermoset components such as microfluidic devices,[1–4] reaction vessels,[5–7] and soft robots[8–12] have been successfully fabricated by stereolithography, digital light processing, inkjet printing, and direct ink writing (DIW), significant challenges remain for rapid fabrication of complex structures with high strength, stiffness, and thermal stability. High-speed printing of complex, high-resolution structures has been achieved through photocuring,[13,14] but the thermomechanical properties are often inferior to thermally cured counterparts. DIW is an extrusion-based technique highly suitable for 3D printing thermally cured thermosets with excellent properties.[15] The ability to add reinforcing fibers and particles further enhances the engineering properties of DIW materials.[16,17] However, the inherent viscoelasticity of DIW inks invariably leads to creep and slumping of deposited structures, especially gap-spanning features, often limiting the size and geometrical complexity of the manufactured part.[11,18–20] More recently, Qi and co-workers combined light- and thermal-curing resins to enable rapid initial solidification by photocuring followed by thermal post-curing to achieve desired engineering properties.[21,22]

An alternative printing approach for thermoset resins relies on frontal polymerization (FP) during DIW to enable rapid curing of printed structures in tandem with the printing process.[23] FP is initiated by a thermal or photo stimulus, triggering an exothermic cure front that propagates by transport of heat and continued reaction in the monomer. During FP-DIW,

J. E. Aw, L. M. Dean, R. H. Ewoldt, P. H. Geubelle, N. R. Sottos
Beckman Institute for Advanced Science and Technology
University of Illinois at Urbana-Champaign
Urbana, IL 61801, USA
E-mail: geubelle@illinois.edu; n-sottos@illinois.edu
J. E. Aw, P. H. Geubelle
Department of Aerospace Engineering
University of Illinois at Urbana-Champaign
Urbana, IL 61801, USA

The ORCID identification number(s) for the author(s) of this article can be found under https://doi.org/10.1002/admt.202200230.

DOI: 10.1002/admt.202200230

X. Zhang
Department of Mechanical Engineering
University of Wyoming
Laramie, WY 82071, USA
A. Z. Nelson
Food, Chemical and Biotechnology Center
Singapore Institute of Technology
Singapore 138683, Singapore
L. M. Dean, N. R. Sottos
Department of Materials Science and Engineering
University of Illinois at Urbana-Champaign
Urbana, IL 61801, USA
M. Yourdkhani
Department of Mechanical Engineering
Colorado State University
Fort Collins, CO 80523, USA
R. H. Ewoldt
Department of Mechanical Engineering
University of Illinois at Urbana-Champaign
Urbana, IL 61801, USA

a monomeric ink is cured by the self-sustaining reaction front upon extrusion. Concurrent polymerization of the filament during extrusion enables layer-by-layer as well as free-form DIW. Freestanding thermoset structures with high strength, stiffness, and glass transition temperature are fabricated without any postcure. Like other DIW methods, reinforcing fillers can be incorporated into the ink to produce functional composites.[24–27]

Coordinating deposition speed to the cure kinetics during FP-DIW is a challenging optimization problem. In our initial study,[23] the cure front was thought to be independent of the printing process and the print speed needed to match the front speed at all times, severely limiting the process. While processing maps or models can guide the selection of optimal printing parameters, [18,20,21,28–34] this open-loop calibrate-then-print approach is only efficient for simple print geometries. The printing of complex geometries requires continuous closed-loop feedback between cure kinetics and deposition speed while accounting for all relevant parameters in a dynamic workspace.[35] Current strategies to achieve closed-loop feedback during printing rely on a combination of sensors to receive real-time process information and artificial intelligence (AI) to compute and implement corrections. Closed-loop feedback has led to reported improvements in printing precision,[36–40] minimization of defects,[41,42] and the ability to print accurately on moving surfaces.[43,44] To date, the correction times for most of these computerized systems are relatively slow, of the order of 10 s,[35] and the use of sensors generates additional challenges pertaining to their accuracy and embedment. While closed-loop feedback is effective at improving issues of inconsistent quality, its use is absent in 3D printing platforms due to multiple implementation difficulties.

Here, we demonstrate the self-regulative control of FP-DIW through the inherent coupling of the frontal curing and deposition processes, without the need for sensors or AI. Contrary to our earlier study, we find that the Arrhenius reaction kinetics (dependence of the polymerization front on initial resin temperature) of the curing reaction is coupled to the printing mechanics, creating a self-regulatory mechanism that synchronizes the front speed to the nozzle printing speed automatically and enabling printing of high fidelity, complex architectures that are not accessible through other DIW approaches. We also model the underlying thermo-chemical processes key to the speed-regulating mechanism to predict and better understand the dynamic front response.

2. Results and Discussion

The FP-DIW process is summarized in **Figure 1**a. A gelled monomeric ink is stored at a temperature of about −5 °C in a chilled ink barrel and is extruded through a printhead. As filaments are deposited on a heated print bed, the available heat initiates a self-propagating cure front along the filament. The ink barrel is kept at −5 °C to mitigate background polymerization, minimize changes in the ink rheology, and extend working time. The cold metal nozzle also consistently quenches the reaction front, eliminating clogging issues in the nozzle and providing a convenient way to terminate a print path.

For the ink, we exploit the frontal ring-opening metathesis polymerization of dicyclopentadiene (DCPD; Figure 1b),[45–47] although FP has been demonstrated in other thermosetting resins such as epoxies,[48–50] polyurethane,[51,52] and polyacrylates.[53,54] Gradual gelation of the DCPD resin is achieved through the addition of a ruthenium catalyst ([Ru]) and a tributyl phosphite (TBP) inhibitor to the DCPD resin.[23] After sufficient time, a partially cured, viscoelastic gel is formed (Figures S1 and S2, Supporting Information) with the requisite rheology for printing. As shown in Figure 1c, the DCPD ink exhibits shear thinning necessary for controlled extrusion.[55–58] The filament retains its extruded shape for several seconds before deforming (Figure S3, Supporting Information). The time scale associated with filament relaxation must be longer than the cure time to ensure fidelity of the printed shape. The gelled DCPD ink takes 20 s to completely relax at the ambient print temperature of 20 °C (Figure 1d), which is sufficient since the front typically catches up with the printhead within 5 s. The ink rheology at the barrel temperature (−5 °C) is also shown in Figure 1c,d for completeness. High extensibility of the ink is also desirable to prevent filaments from rupturing when stretched or bent, especially when free-form printing with no support structures.[59,60] As annotated in Figure 1e, the extensional failure strain of our DCPD ink is ≈1200%. This remarkable strain-to-failure is attributed to the relatively high molar mass of the ink and resulting polymer chain entanglements (Figure S1b, Supporting Information).

Upon printing a single filament on a print bed heated to ≈100 °C, we tracked the exothermic front using IR imaging. A representative IR image is shown in **Figure 2**a. When the speed of the nozzle, V_{print}, is set to 1.2 mm s^{-1}, the propagating front decelerates from about 1.7 to 1.2 mm s^{-1} (Figure 2c; Video S1, Supporting Information). Increasing the print speed V_{print} to 2.6 mm s^{-1} while keeping all other process parameters (temperature of heated substrate and extrusion flow rate) unchanged causes the polymerization front to accelerate and then stabilize to the prescribed print speed (Figure 2d; Video S1, Supporting Information). This self-regulative behavior of the cure front was observed over the range 1.2 mm $s^{-1} \leq V_{print} \leq 3.0$ mm s^{-1}.

Computational modeling of the coupled reaction-diffusion relations that govern FP[23,61] predicts that the front speed increases with the initial temperature of the gel (solid curve in Figure 2b, details provided in Supporting Information Section S3.3). To verify the dependence of front speed on the gel temperature, we also measured two additional parameters: the length L of the uncured filament, i.e., the distance between the nozzle and the polymerization front, and the gel temperature T_{gel} at the arrival of the front (Figure 2a). The relationship between T_{gel} and V_{front} was also obtained empirically (symbols and dashed curve in Figure 2b).

The self-regulative front speed is due to a mechanism similar to closed-loop feedback but based on the filament heating from the print environment and temperature dependence of the front speed. When the front travels faster than the nozzle ($V_{front} > V_{print}$), the front gets closer to the nozzle (i.e., L decreases) toward the cooler regions of the filament. As the front encounters gel filament of lower temperature, the cure front decelerates, as shown by the decrease in V_{front} in Figure 2c. In contrast, if the front propagates slower than the printing nozzle ($V_{front} < V_{print}$), it increasingly lags behind

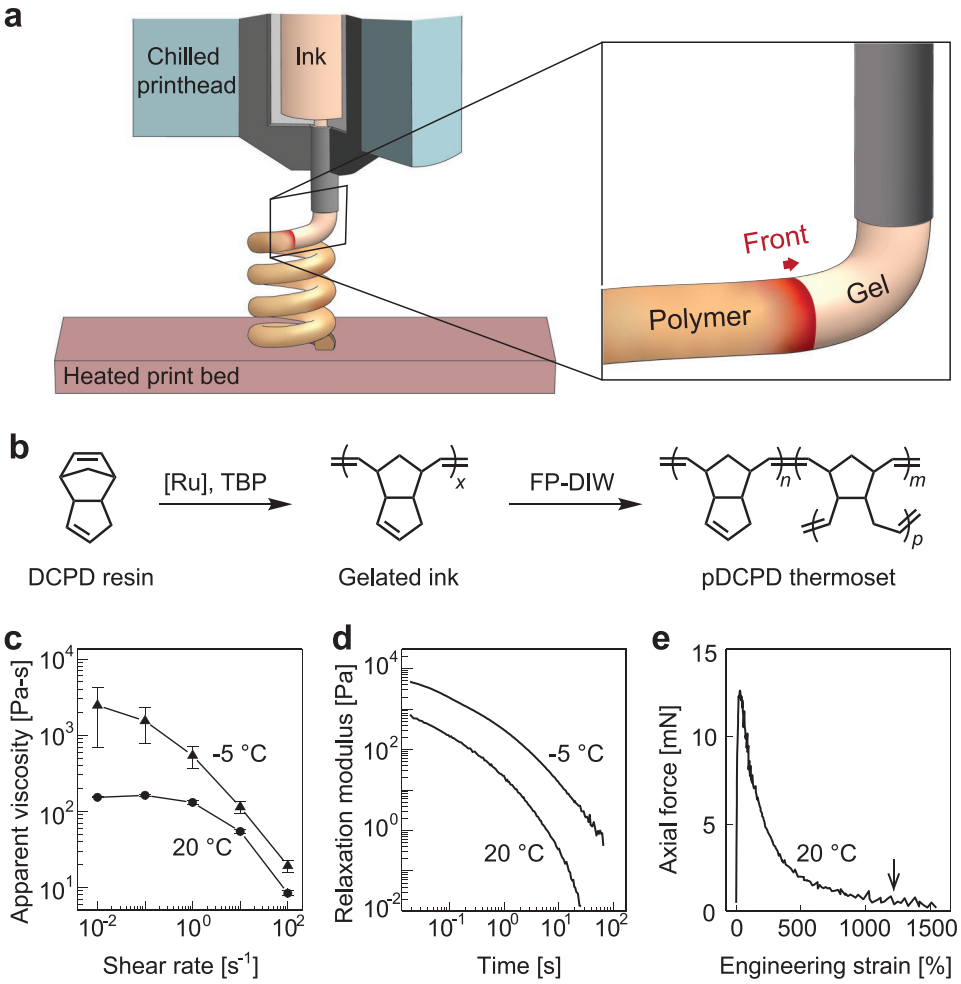

Figure 1. Frontal-polymerization-enabled DIW process for thermoset polymers. a) Schematic of cure front propagation during extrusion of gelled ink from the chilled printhead (–5 °C). The heated print bed (≈100 °C) initiates a self-propagating front, enabling the printing of complex structures. b) Chemical scheme for gelation of DCPD monomer into a printable ink and the frontal polymerization during DIW. c–e) Key rheological properties for printing ink include c) shear-thinning flow, d) a moderate relaxation behavior, and e) a high extensional failure strain (failure is indicated by the arrow).

the nozzle (i.e., L increases), retreating to a higher temperature region of the deposited filament. Due to the monotonic relation between front speed and gel temperature in Figure 2b, the falling back of the front subsequently leads to front acceleration, as depicted in Figure 2d. Continuous readjustments of the front-nozzle distance due to front acceleration/deceleration creates a self-restoring dynamic that allows the front speed to progressively self-correct toward V_{print} in both situations.

The self-regulating process is thus the result of a reaction-diffusion process that links the front speed to the temperature of the gel, the progressive heating of the deposited material over the length L of the uncured filament (Figure S5, Supporting Information), and the kinematics that describes the time evolution of L. In its simplest form, the model can be schematically described by **Figure 3**. In addition to the monotonic T_{gel}–V_{front} relation shown in Figure 2b, the model involves the following expression for the evolution of L:

$$L = L_0 + \int_0^t \left[V_{print} - V_{front} \right] d\tau \tag{1}$$

where L_0 is the initial value of L when the polymerization front is initiated. The progressive heating of the deposited gel due to both conduction and convection can be modeled by

$$T_{gel} = T_\infty - (T_d - T_\infty) \exp\left(\frac{-4h}{\rho c_p D} t_{expose} \right) \tag{2}$$

where T_d is the deposited temperature at extrusion, T_∞ is the surrounding temperature, h is the equivalent heat transfer coefficient between the filament and environment, ρ and c_p respectively denote the density and specific heat capacity of the gel, and D is the filament diameter. t_{expose}, defined as the exposure time to the print environment, can be simplified as L/V_{print}. The derivation of the Equation (2) is provided in Supporting Information Section S3.2. As reflected in the red curves in Figure 2c,d, this simple model captures well the front deceleration and acceleration as well as the stable plateau at $V_{front} = V_{print}$. Good agreement is also obtained between predicted and measured values of T_{gel} and L, further validating the proposed mechanism.

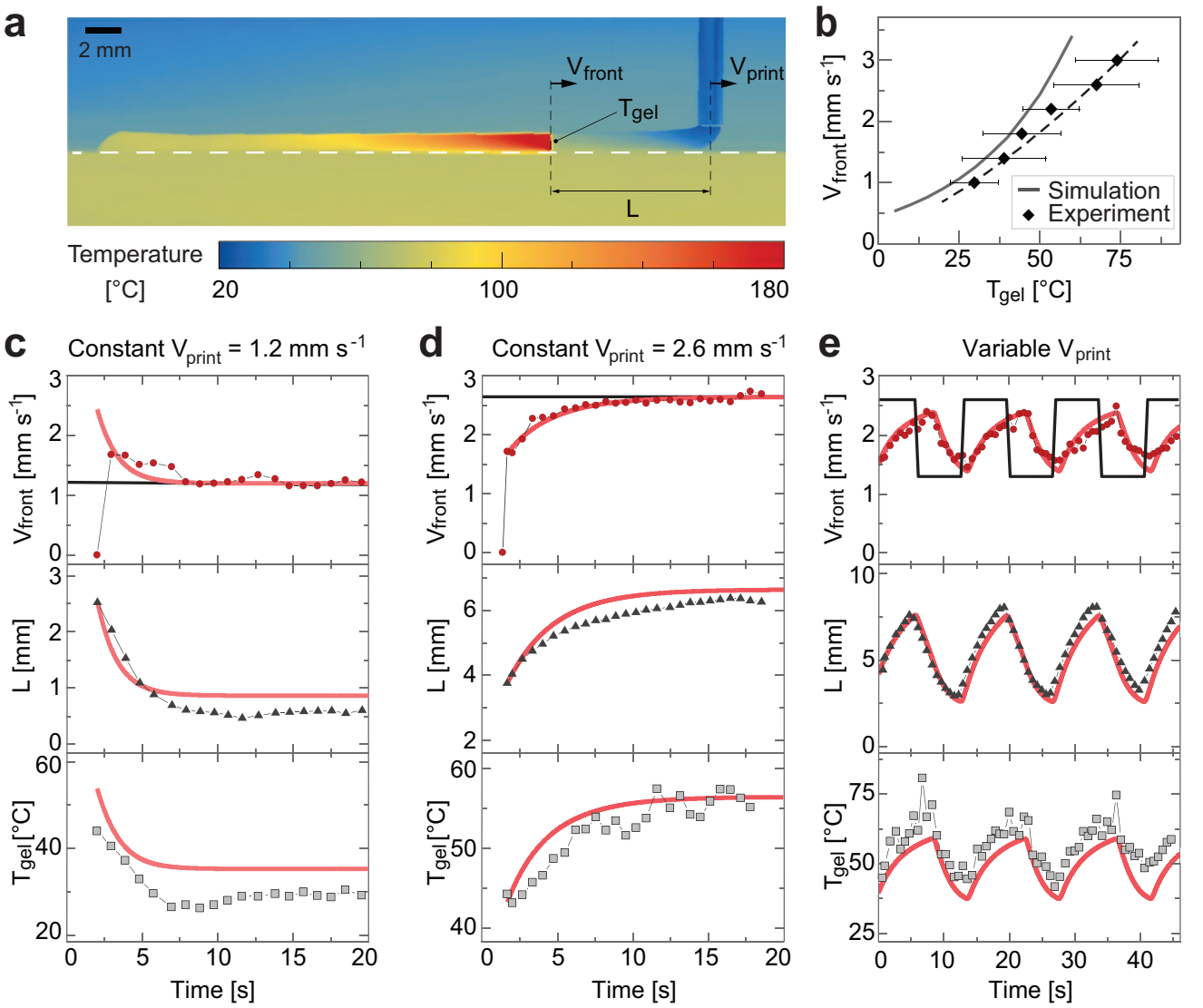

Figure 2. Experimental demonstration and modeling of the self-regulative mechanism during FP-DIW. a) Representative IR snapshot during the printing process. The speed of the print nozzle is set at V_{print} and T_{gel} is the temperature of the gel measured just behind the cure front, which moves at speed V_{front} and lags behind the nozzle at distance L. The dashed white line indicates the location of the top edge of the print bed. b) V_{front} as a function of the initial temperature of the gel. Horizontal error bars represent standard deviation from the mean ($n \geq 4$), while vertical error bars are negligibly small. Self-regulative response to c) constant $V_{print} = 1.2$ mm s^{-1}, d) constant V_{print} of 2.6 mm s^{-1}, and e) for variable V_{print}. The imposed value of V_{print} is denoted by the solid black line in the top row figures. The symbols and red curves respectively denote the measured and predicted evolution of the V_{front} (top row), L (middle row), and T_{gel} (bottom row).

The natural coupling of the frontal response to the printing speed is further demonstrated for the case of alternating print speeds in Figure 2e. The front rapidly senses changes in the printing conditions and adapts its behavior through acceleration or deceleration. The front responds within 1 s when L is small (≈2 mm), but the response time is extended to 4 s for larger values of L (≈7 mm) due to a longer catch-up distance for the front. The evolutions of V_{front}, L, and T_{gel} along with the different response times are well reproduced by the transient model. Considering that heat is transferred from the surroundings to the filament, the temperature of the heating bed sets the upper limit for T_{gel} and, thereby for V_{front}. The key element to replicating the self-regulative mechanism is the Arrhenius-type reaction kinetics (i.e., the dependence of front speed on the material temperature), which has been reported for a number of frontally polymerizing materials.[62–66] Therefore, we anticipate the self-regulative mechanism observed here for DCPD resin will likely occur in other frontally polymerizing thermosets, provided that the environment temperature is suitably controlled within the active temperature range for FP.

Similar to many self-regulating engineering systems, the FP-DIW process demonstrates an inherent resilience to changes in external conditions.[67–71] Lowering the ambient temperature (T_∞) should lead to a decrease in front speed,[61] yet we observe that the system is able to self-correct in response to different T_∞ values, similar to the response to changes in V_{print}.

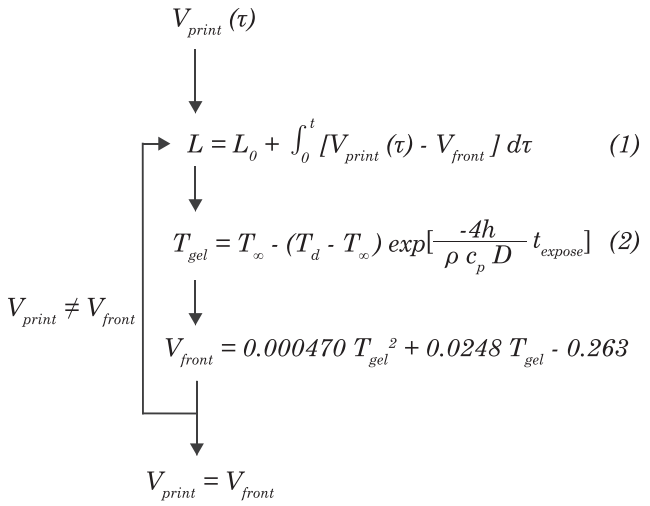

Figure 3. Algorithm for the computational model. The model connects physical parameters L, T_{gel}, and V_{front} together into a reciprocating loop. L, T_{gel}, and V_{front} continuously adjust when $V_{front} \neq V_{print}$ until the value of V_{front} reaches an equilibrium with V_{print}.

As T_∞ is decreased from 100 to 60 °C, an initial front deceleration is observed (Figure S7, Supporting Information), followed by a self-correction to equilibrate the front speed once again to the print speed. A similar self-correction was captured during the transition between printing on heated support and printing in midair (Figure S8, Supporting Information). Adapting to variable thermal conditions is advantageous since environmental temperature may change during the printing process.

The self-regulating front produces prints with excellent quality. The printed pDCPD filaments are fully cured (α = 0.98), exhibiting a high Young's Modulus (E = 1.9 ± 0.1 GPa) and yield strength (σ_y = 51.8 ± 1.7 MPa) (Figure S9 and Table S2, Supporting Information). The production of high-fidelity structures requires minimal sagging deformation along the viscoelastic uncured portion L of the filament.[28] Choosing print speeds that maintain L at ≈4 mm or less enables free-form printing of complex curvilinear features without support. The printed overhanging beams in **Figure 4**a and cantilevers in Figure 4b exhibit cross-sections with high circularity. No viscoelastic sag is observed during the printing of the filaments (Video S2, Supporting Information), and the tip-end deflections for the cantilevered filaments compare well with predictions obtained for linearly elastic Euler-Bernoulli cantilever beams (Figure 4c,d). These load-supporting filaments easily spanned across a 100 mm gap. This is a significant advance over prior reports of DIW that produced a maximum of 20 mm spans.[19,21,28,31,59,74] The minimum filament diameter is currently limited to ≈400 µm due to quenching of FP from heat loss in thinner filaments. Smaller filaments could be achieved by printing at a higher ambient temperature or using alternative resins with greater exotherms and heat release rates, such as exo-DCPD.[72] Moreover, printing at variable speeds (while keeping the material extrusion rate constant) will cause the filament to stretch and potentially enable control of diameter on-the-fly.[73]

To further demonstrate the capabilities of FP-DIW, we fabricated several complex free-form structures that are difficult

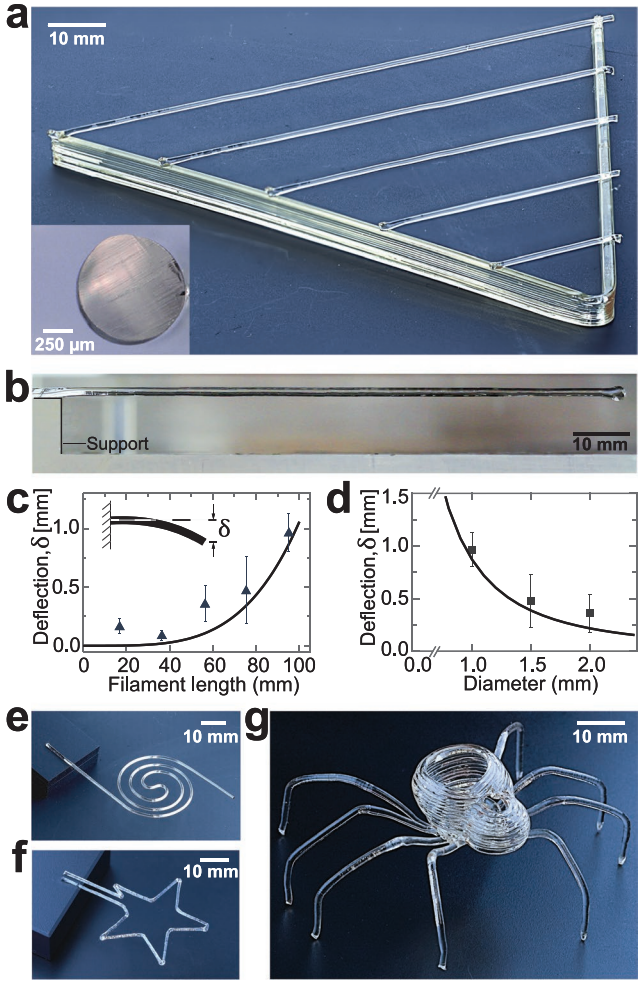

Figure 4. FP-DIW of freestanding architectures. a) Overhanging beams (with diameter D = 1 mm) were printed across 20, 40, 60, 80, and 100 mm spans in the absence of supports (V_{print} = 1.0 mm s^{-1}). Inset shows the circular filament cross-section. b) Representative printed cantilever beam (V_{print} = 1.1 mm s^{-1}), with the black solid line outlining the edges of the support ledge. Measured tip-end deflection δ (symbols) and prediction from Euler-Bernoulli beam theory (solid curve) as a function of c) printed cantilever beam length for a 1 mm filament diameter, and d) filament diameter for a cantilever beam length of 100 mm. Error bars represent the standard deviation from the mean ($n \geq 3$). Examples of complex features printed with FP-DIW: e) cantilevered Fermat spiral (V_{print} = 1.3 mm s^{-1}), f) cantilevered star (V_{print} = 1.0 mm s^{-1}), g) spider created by a combination of free-form and layer-by-layer FP-DIW (1.3 mm s^{-1} ≤ V_{print} ≤ 1.8 mm s^{-1}). All structures are fabricated on a 100 °C print bed.

to produce using conventional DIW (Figure 4e–g). The Fermat spiral in Figure 4e showcases the ability to create precise curvatures in midair. Deviations between the toolpath and printed structure are minimal (Figure S10, Supporting Information). Restricting L ($L \leq 4$ mm)[28,32] aligns the filament better with the curvature tangents and results in precise curvatures (Figure S11, Supporting Information). As the print speed increases, keeping L large would lead to poor shape replication; a failed specimen is shown in Figure S11b in the Supporting Information. The rapid deceleration of the print head brings the front even closer to the nozzle and translates to even smaller values of L (≈1 mm). Momentarily pausing the print nozzle creates the

corner features shown in Figure 4f. As a final demonstration of the printing ability, we built a spider spanning over 80 mm in width (Figure 4g). The spider legs were printed first before constructing a body layer-by-layer directly on top of the legs (Figure S12, Supporting Information).

3. Conclusion

In this work, we have demonstrated the direct ink writing of complex structures enabled by self-regulating print speed under varying conditions and excellent dimensional stability of the rapidly cured filaments. The mechanism behind self-regulative front behavior is analogous to a closed, continuous feedback loop, enabling the front to sense the printing conditions and rapidly correct its front speed to match the prescribed print velocity. Unlike computerized control systems used with other printing processes, the coupled feedback effects in FP-DIW are integrated in the underlying physics. A computational model was developed to better understand the self-regulating behavior and capture the influence of key process parameters. FP-DIW readily produces high-fidelity free-form and layer-by-layer features with excellent mechanical and thermomechanical properties. This expansion of printing capabilities can be combined with a diverse palette of ink fillers to induce tunable functionality in sophisticated, tailored architectures.

Supporting Information

Supporting Information is available from the Wiley Online Library or from the author.

Acknowledgements

The authors acknowledge the support from Air Force Office of Scientific Research (AFOSR grant # FA9550-20-1-0194, Center of Excellence Phase II Self-healing to Morphogenic Manufacturing, and the National Science Foundation Grant NSF CMMI 1933932. X.Z. was supported by the faculty start-up funding from the University of Wyoming and a postdoctoral fellowship from the University of Illinois. A.Z.N. acknowledges postdoctoral support from the National Research Foundation, Prime Minister's Office, Singapore under its Campus for Research Excellence and Technological Enterprise (CREATE) program. The authors thank the Beckman Institute for Advanced Science and Technology for their facilities and equipment, and Prof. Jeffrey S. Moore for helpful discussions. The authors also gratefully acknowledge their colleague and mentor Prof. Scott R. White whose visionary ideas inspired this work.

Conflict of Interest

The authors declare no conflict of interest.

Data Availability Statement

The data that support the findings of this study are available from the corresponding author upon reasonable request.

Keywords

3D free-form printing, additive manufacturing, direct ink writing, frontal polymerization, self-regulation, thermosets polymers

Received: March 8, 2022
Published online:

[1] J. L. Sanchez Noriega, N. A. Chartrand, J. C. Valdoz, C. G. Cribbs, D. A. Jacobs, D. Poulson, M. S. Viglione, A. T. Woolley, P. M. Van Ry, K. A. Christensen, G. P. Nordin, *Nat. Commun.* **2021**, *12*, 5509.
[2] Q. Zhang, X. Peng, S. Weng, R. Zhang, D. Fang, R. Zhao, H. J. Qi, *Extreme Mech. Lett.* **2020**, *39*, 100824.
[3] A. K. Au, W. Lee, A. Folch, *Lab Chip* **2014**, *14*, 1294.
[4] N. P. Macdonald, J. M. Cabot, P. Smejkal, R. M. Guijt, B. Paull, M. C. Breadmore, *Anal. Chem.* **2017**, *89*, 3858.
[5] M. D. Symes, P. J. Kitson, J. Yan, C. J. Richmond, G. J. T. Cooper, R. W. Bowman, T. Vilbrandt, L. Cronin, *Nat. Chem.* **2012**, *4*, 349.
[6] C. Y. Chaparro-Garnica, A. Davó-Quiñonero, E. Bailón-García, D. Lozano-Castelló, A. Bueno-López, *ACS Appl. Mater. Interfaces* **2019**, *11*, 36763.
[7] S. Rossi, A. Puglisi, L. M. Raimondi, M. Benaglia, *Catalysts* **2020**, *10*, 109.
[8] M. A. Skylar-Scott, J. Mueller, C. W. Visser, J. A. Lewis, *Nature* **2019**, *575*, 330.
[9] Y. Kim, H. Yuk, R. Zhao, S. A. Chester, X. Zhao, *Nature* **2018**, *558*, 274.
[10] R. L. Truby, M. Wehner, A. K. Grosskopf, D. M. Vogt, S. G. M. Uzel, R. J. Wood, J. A. Lewis, *Adv. Mater.* **2018**, *30*, 1706383.
[11] Q. Zhang, S. Weng, Z. Zhao, H. J. Qi, D. Fang, *Appl. Math. Mech.* **2021**, *42*, 159.
[12] T. J. Wallin, J. H. Pikul, S. Bodkhe, B. N. Peele, B. C. Mac Murray, D. Therriault, B. W. McEnerney, R. P. Dillon, E. P. Giannelis, R. F. Shepherd, *J. Mater. Chem. B* **2017**, *5*, 6249.
[13] J. R. Tumbleston, D. Shirvanyants, N. Ermoshkin, R. Janusziewicz, A. R. Johnson, D. Kelly, K. Chen, R. Pinschmidt, J. P. Rolland, A. Ermoshkin, E. T. Samulski, J. M. DeSimone, *Science* **2015**, *347*, 1349.
[14] M. Regehly, Y. Garmshausen, M. Reuter, N. F. König, E. Israel, D. P. Kelly, C.-Y. Chou, K. Koch, B. Asfari, S. Hecht, *Nature* **2020**, *588*, 620.
[15] V. Ozbolat, M. Dey, B. Ayan, A. Povilianskas, M. C. Demirel, I. T. Ozbolat, *ACS Biomater. Sci. Eng.* **2018**, *4*, 682.
[16] B. G. Compton, J. A. Lewis, *Adv. Mater.* **2014**, *26*, 5930.
[17] J. P. Lewicki, J. N. Rodriguez, C. Zhu, M. A. Worsley, A. S. Wu, Y. Kanarska, J. D. Horn, E. B. Duoss, J. M. Ortega, W. Elmer, R. Hensleigh, R. A. Fellini, M. J. King, *Sci. Rep.* **2017**, *7*, 43401.
[18] J. Zhu, Q. Zhang, T. Yang, Y. Liu, R. Liu, *Nat. Commun.* **2020**, *11*, 3462.
[19] J. E. Smay, J. Cesarano, J. A. Lewis, *Langmuir* **2002**, *18*, 5429.
[20] L. L. Lebel, B. Aissa, M. A. E. Khakani, D. Therriault, *Adv. Mater.* **2010**, *22*, 592.
[21] K. Chen, X. Kuang, V. Li, G. Kang, H. J. Qi, *Soft Matter* **2018**, *14*, 1879.
[22] X. Kuang, Z. Zhao, K. Chen, D. Fang, G. Kang, H. J. Qi, *Macromol. Rapid Commun.* **2018**, *39*, 1700809.
[23] I. D. Robertson, M. Yourdkhani, P. J. Centellas, J. E. Aw, D. G. Ivanoff, E. Goli, E. M. Lloyd, L. M. Dean, N. R. Sottos, P. H. Geubelle, J. S. Moore, S. R. White, *Nature* **2018**, *557*, 223.
[24] L. M. Dean, A. Ravindra, A. X. Guo, M. Yourdkhani, N. R. Sottos, *ACS Appl. Polym. Mater.* **2020**, *2*, 4690.
[25] S. C. Leguizamon, A. W. Cook, L. N. Appelhans, *Chem. Mater.* **2021**, *33*, 9677.

[26] R. D. Farahani, M. Dubé, D. Therriault, *Adv. Mater.* **2016**, *28*, 5794.
[27] W. Xu, S. Jambhulkar, D. Ravichandran, Y. Zhu, M. Kakarla, Q. Nian, B. Azeredo, X. Chen, K. Jin, B. Vernon, D. G. Lott, J. L. Cornella, O. Shefi, G. Miquelard-Garnier, Y. Yang, K. Song, *Small* **2021**, *17*, 2100817.
[28] R. D. Farahani, L. L. Lebel, D. Therriault, *J. Micromech. Microeng.* **2014**, *24*, 055020.
[29] K. Tian, J. Bae, S. E. Bakarich, C. Yang, R. D. Gately, G. M. Spinks, M. in het Panhuis, Z. Suo, J. J. Vlassak, *Adv. Mater.* **2017**, *29*, 1604827.
[30] J. Wang, R. C. Y. Auyeung, H. Kim, N. A. Charipar, A. Piqué, *Adv. Mater.* **2010**, *22*, 4462.
[31] S. Bodkhe, G. Turcot, F. P. Gosselin, D. Therriault, *ACS Appl. Mater. Interfaces* **2017**, *9*, 20833.
[32] M. A. Skylar-Scott, S. Gunasekaran, J. A. Lewis, *Proc. Natl. Acad. Sci.* **2016**, *113*, 6137.
[33] S.-Z. Guo, F. Gosselin, N. Guerin, A.-M. Lanouette, M.-C. Heuzey, D. Therriault, *Small* **2013**, *9*, 4118.
[34] S.-Z. Guo, M.-C. Heuzey, D. Therriault, *Langmuir* **2014**, *30*, 1142.
[35] Z. Zhu, D. W. H. Ng, H. S. Park, M. C. McAlpine, *Nat. Rev. Mater.* **2021**, *6*, 27.
[36] P. Sitthi-Amorn, J. E. Ramos, Y. Wang, J. Kwan, J. Lan, W. Wang, W. Matusik, *ACM Trans. Graph.* **2015**, *34*, 129.
[37] E. Barnett, C. Gosselin, *Addit. Manuf.* **2015**, *7*, 27.
[38] K. Cui, X. Shang, C. Luo, Z. Shen, H. Gao, G. Xiong, in *2019 IEEE Int. Conf. Serv. Oper. Logist. Inform. SOLI*, IEEE, Zhengzhou, China, **2019**, pp. 5–9.
[39] Yu. G. Kabaldin, P. V. Kolchin, D. A. Shatagin, M. S. Anosov, A. A. Chursin, *Russ. Eng. Res.* **2019**, *39*, 848.
[40] K. Garanger, T. Khamvilai, E. Feron, in *2018 IEEE Conf. Control Technol. Appl. CCTA*, IEEE, Copenhagen **2018**, pp. 465–470.
[41] Z. Jin, Z. Zhang, G. X. Gu, *Manuf. Lett.* **2019**, *22*, 11.
[42] B. Panda, J. H. Lim, N. A. Noor Mohamed, S. C. Paul, Y. W. D. Tay, M. J. Tan, in *34th International Symposium on Automation and Robotics in Construction*, Taipei, Taiwan **2017**.
[43] Z. Zhu, S.-Z. Guo, T. Hirdler, C. Eide, X. Fan, J. Tolar, M. C. McAlpine, *Adv. Mater.* **2018**, *30*, 1707495.
[44] Z. Zhu, H. S. Park, M. C. McAlpine, *Sci. Adv.* **2020**, *6*, eaba5575.
[45] A. Mariani, S. Fiori, Y. Chekanov, J. A. Pojman, *Macromolecules* **2001**, *34*, 6539.
[46] A. Ruiu, D. Sanna, V. Alzari, D. Nuvoli, A. Mariani, *J. Polym. Sci. A: Polym. Chem.* **2014**, *52*, 2776.
[47] I. D. Robertson, L. M. Dean, G. E. Rudebusch, N. R. Sottos, S. R. White, J. S. Moore, *ACS Macro Lett.* **2017**, *6*, 609.
[48] A. Mariani, S. Bidali, S. Fiori, M. Sangermano, G. Malucelli, R. Bongiovanni, A. Priola, *J. Polym. Sci. A: Polym. Chem.* **2004**, *42*, 2066.
[49] Y. Chekanov, D. Arrington, G. Brust, J. A. Pojman, *J. Appl. Polym. Sci.* **1997**, *66*, 1209.
[50] Z. Zhang, R. Liu, W. Li, Y. Liu, H. Luo, L. Zeng, J. Qiu, S. Wang, *Addit. Manuf.* **2021**, *47*, 102348.
[51] S. Fiori, A. Mariani, L. Ricco, S. Russo, *Macromolecules* **2003**, *36*, 2674.
[52] A. Mariani, S. Bidali, S. Fiori, G. Malucelli, E. Sanna, *E-Polym.* **2003**, *3*, 044.
[53] C. Nason, T. Roper, C. Hoyle, J. A. Pojman, *Macromolecules* **2005**, *38*, 5506.
[54] S. Chen, T. Hu, Y. Tian, L. Chen, J. A. Pojman, *J. Polym. Sci. A: Polym. Chem.* **2007**, *45*, 873.
[55] H. A. Barnes, *A Handbook of Elementary Rheology*, Univ. Of Wales, Institute Of Non-Newtonian Fluid Mechanics, Aberystwyth, **2000**.
[56] R. L. Truby, J. A. Lewis, *Nature* **2016**, *540*, 371.
[57] D. Therriault, S. R. White, J. A. Lewis, *Appl. Rheol.* **2007**, *17*, 10112.
[58] A. Z. Nelson, K. S. Schweizer, B. M. Rauzan, R. G. Nuzzo, J. Vermant, R. H. Ewoldt, *Curr. Opin. Solid State Mater. Sci.* **2019**, *23*, 100758.
[59] B. M. Rauzan, A. Z. Nelson, S. E. Lehman, R. H. Ewoldt, R. G. Nuzzo, *Adv. Funct. Mater.* **2018**, *28*, 1707032.
[60] A. Z. Nelson, R. E. Bras, J. Liu, R. H. Ewoldt, *J. Rheol.* **2018**, *62*, 357.
[61] E. Goli, T. Gai, P. H. Geubelle, *J. Phys. Chem. B* **2020**, *124*, 6404.
[62] A. Kumar, Y. Gao, P. H. Geubelle, *J. Polym. Sci.* **2021**, *59*, 1109.
[63] P. M. Goldfeder, V. A. Volpert, V. M. Ilyashenko, A. M. Khan, J. A. Pojman, S. E. Solovyov, *J. Phys. Chem. B* **1997**, *101*, 3474.
[64] I. P. Nagy, L. Sike, J. A. Pojman, *J. Am. Chem. Soc.* **1995**, *117*, 3611.
[65] A. O. Tonoyan, S. P. Davtyan, S. C. Müller, *Macromol. React. Eng.* **2014**, *8*, 442.
[66] Q.-Z. Yan, W.-F. Zhang, G.-D. Lu, X.-T. Su, C.-C. Ge, *Chem. Eur. J.* **2006**, *12*, 3303.
[67] X. He, M. Aizenberg, O. Kuksenok, L. D. Zarzar, A. Shastri, A. C. Balazs, J. Aizenberg, *Nature* **2012**, *487*, 214.
[68] B. Hatton, L. Mishchenko, S. Davis, K. H. Sandhage, J. Aizenberg, *Proc. Natl. Acad. Sci.* **2010**, *107*, 10354.
[69] M. M. Lerch, A. Grinthal, J. Aizenberg, *Adv. Mater.* **2020**, *32*, 1905554.
[70] D. T. Eddington, R. H. Liu, J. S. Moore, D. J. Beebe, *Lab Chip* **2001**, *1*, 96.
[71] D. Martella, S. Nocentini, C. Parmeggiani, D. S. Wiersma, *Adv. Mater. Technol.* **2018**, *4*, 1800571.
[72] I. D. Robertson, E. L. Pruitt, J. S. Moore, *ACS Macro Lett.*. **2016**, *5*, 593.
[73] H. Yuk, X. Zhao, *Adv. Mater.* **2018**, *30*, 1704028.
[74] S. Gantenbein, C. Mascolo, C. Houriet, R. Zboray, A. Neels, K. Masania, A. R. Studart, *Adv. Funct. Mater.* **2021**, *31*, 2104574.